Direct Measurement of Inter-Filament Resistance in Superconducting Multifilamentary NbTi and Nb_3Sn Strands

C. Zhou, E. P. A. van Lanen, D. Veldhuis, H. H. J. ten Kate, M. Dhallé, and A. Nijhuis

***Abstract*—A quantitative knowledge of inter-filament transverse resistance will allow us to describe current redistribution processes inside strands more accurately. This is particularly important for the analysis of the influence of strain and crack distribution patterns in Nb_3Sn filaments on the shape of the voltage-current curves. Several indirect methods are commonly used to assess inter-filament resistance. Here we use a direct method to measure transverse inter-filament resistance and filament-to-matrix contact resistance. Two four-probe voltage-current methods are developed for measurements below 10 K at various background magnetic fields. In addition to FEM (Finite Element Method) simulation, also a new 3D strand model is developed to simulate the current- and voltage distributions. The experimental methods, first results as well as the simulations using the FEM method and new 3D strand model are described.**

***Index Terms*—Current distribution, inter-filament resistance, NbTi, Nb_3Sn, proximity effect, 3D strand model.**

I. Introduction

Superconducting wires with many fine filaments in a stabilizing matrix are commonly used in cable-in-conduit conductors (CICC), as applied to the magnets in the International Thermonuclear Experimental Reactor (ITER). Inter-filament transverse resistance plays an important role in AC coupling loss and in current redistribution processes inside strands [1], [2], e.g. determining the shape of the V–I curves in strained and/or cracked Nb_3Sn filaments [3]. When Nb_3Sn type CICCs are mechanically loaded, the axial and transverse strain in the filamentary region varies spatially. In severe loading cases, the same occurs for cracks that are initiated in the filaments when the irreversibility limit is exceeded.

Several methods were developed to assess the inter-filament transverse resistance, such as measurements of the self-field distribution [4], [5]; of the AC coupling losses at low frequency [3], [6], [7]; and of the current transfer length [8]. However, the outcome of these indirect measurement methods depends on sample shape, internal wire structure, outer copper shell, Cu/nonCu ratio and twist pitch [9]. They yield an average transverse resistivity of the combined matrix resistance and matrix/filament contact resistance, however, without details about the precise current distribution among filaments and matrix.

Recently, the inter-filament resistance was measured directly for the first time by V. Corato *et al.*, who used a four-probe configuration with micro-bonded contacts to obtain an effective transverse resistivity [10]. In this work we present two new four-probe voltage-current methods that allow the measurement of inter-filament transverse resistance inside multifilamentary NbTi and Nb_3Sn stands with improved resolution. To aid experimental analysis, a COMSOL FEM model and a new 3D MatLab strand model are developed to simulate the measurements and to extract the filament-to-matrix resistivity.

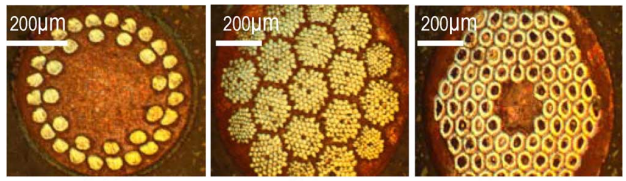

Fig. 1. Cross-sectional photos of the investigated strands.

II. Experimental Setup

The cross-section and characteristics of the three investigated wires are shown in Fig. 1 and Table I. The JT strand is a candidate strand for the JT-60-SA CIC-conductor. The OST Nb_3Sn strand [11], used for the EDIPO dipole coil presently under construction, has 84 bundles with 104 fine filaments per bundle that are proximity coupled and interlinked by sintering. The value of the average transverse resistivity $\rho_\perp$ in Table I is determined from AC coupling loss measurements.

The new experiments are of the classical four-probe voltage-current type. The first setup, called Extracted Filament Setup, is suitable for NbTi strands such as VAC-20-1 in Fig. 1, with a relatively small number of strong and ductile filaments with a large diameter.

After removing the insulation layer and matrix (by wet etching) over a few mm and cutting away most of the exposed filaments, only 3 to 6 filaments are left "sticking out" (Fig. 2) to be used as probes to measure the inter-filament resistance in the remaining un-etched sample section.

Manuscript received August 03, 2010; accepted September 27, 2010. Date of publication November 11, 2010; date of current version May 27, 2011.

C. Zhou, E. P. A. van Lanen, M. Dhallé, and A. Nijhuis are with the Energy, Materials and Systems Group, Faculty of Science and Technology, and the IMPACT Research Institute, University of Twente, 7500 AE Enschede, The Netherlands (e-mail: C.Zhou@tnw.utwente.nl).

H. H. J. ten Kate is with the Energy, Materials and Systems Group, Faculty of Science and Technology, and the IMPACT Research Institute, University of Twente, 7500 AE Enschede, The Netherlands and also with CERN, 1211 Geneva, Switzerland (e-mail: Herman.TenKate@cern.ch).

D. Veldhuis is with the Interfaces and Correlated Electron Systems (ICE) Group and the MESA+ Research Institute, University of Twente, 7500 AE Enschede, The Netherlands.

Color versions of one or more of the figures in this paper are available online at http://ieeexplore.ieee.org.

Digital Object Identifier 10.1109/TASC.2010.2083619

TABLE I
STRAND CHARACTERISTICS

Sample	VAC-20-1	JT-60-SA	OST-EDIPO
superconductor	NbTi	NbTi	Nb_3Sn
Producer	VAC[1)]	Luvata	OST [2)]
Number of filaments	36	1189	8712
Diameter of filaments (μm)	41	20	3
Twist pitch (mm)	50	16	15
Matrix	Cu	Cu	Cu
resistivity $\rho_{\perp\text{-AC}}$ (Ωm)	3.61×10^{-10}	1.37×10^{-10}	2.75×10^{-10}

1) VAC is produced by Vacuumschmelze GmbH (1988), now Bruker-EST
2) OST is Oxford Superconducting Technology

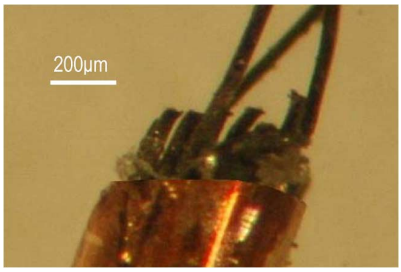

Fig. 2. Extracted filaments (top) and intact wire section (bottom) in the first experiment.

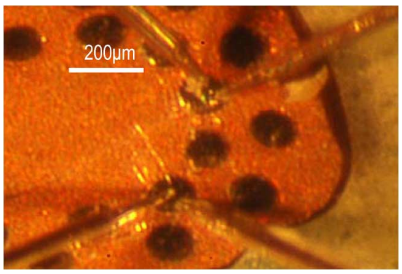

Fig. 3. Measured strand with 4 point contact needles (diameter of tip and top is 8 and 0.1 μm) in the second experiment.

For accurate measurements, the length of the remaining section is limited to 1.5 mm to reach a sufficiently high inter-filament resistance. The end of this section is carefully polished and etched for several seconds to avoid undesired superconducting short circuits caused by filament contacts. Then the sample is mounted on a G10 plate and the filaments sticking out are mechanically fixed. Each filament is connected to a current lead and voltage tap and combinations are measured in liquid helium.

For the NbTi and Nb_3Sn strands with thinner filaments, the Point Contact Setup with 4 micro-contact needles shown in Fig. 3 is used. The polished wire section has a disc shape with a length as short as 10–20 μm. The samples are mounted on an electrically insulated holder, glued to a copper plate with a permanent magnet attached to it. The magnet serves to suppress the proximity effect in the case of small filament spacing [12].

The sample is conduction-cooled below 10 K. A Cernox thermometer attached near the sample monitors the temperature and for control a heater is installed on the cooling plate. The needles

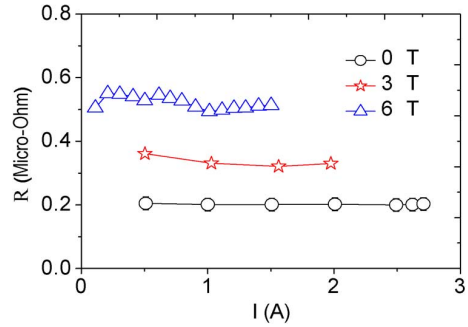

Fig. 4. Inter-filament resistance versus current of sample VAC at 4.2 K.

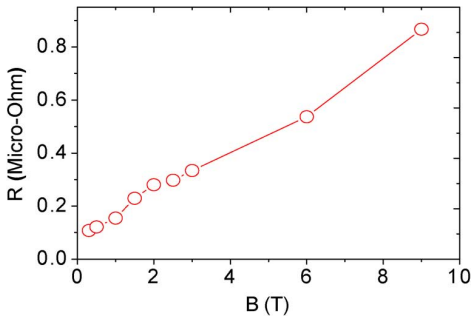

Fig. 5. Inter-filament resistance vs. magnetic field of sample JT-60-SA at 4.2 K.

can be positioned anywhere in the wire cross section, in-situ observed through a microscope, and serve as voltage taps and current leads for the V–I measurements. The Extracted Filament Setup serves to crosscheck and validate the Point Contact Setup.

III. EXPERIMENTAL RESULTS

A. Experimental Results With Extracted Filament Setup

The inter- filament resistance for samples VAC and JT-60-SA, calculated from the V–I data at 4.2 K and a sample length of 1.5 ± 0.1 mm, is shown in Figs. 4 and 5.

A clear ohmic behavior is observed for this straightforward measurement method of interfilament resistance at low current. The slight fluctuation of resistance versus current in a magnetic field of 6 T in Fig. 4 may be related to the Lorentz force on the extracted filament. For the 1.5 mm long VAC sample with the relatively simple cross-sectional geometry, the inter-filament resistance is 2.07×10^{-7} Ω at 4.2 K and 0 T, increasing due to matrix magneto-resisitivity in an external magnetic field. Also for the JT-60-SA wire an increasing inter-filament resistance with applied magnetic field is found.

B. Experimental Results With Point Contact Setup

The inter-filament resistances of VAC and OST strands, determined with the second method on a 23 ± 2 μm long sample. are shown in Fig. 6. The rise of inter-filament resistance with increasing current is likely caused by a rise in temperature at the contact between needle and filament due to ohmic heating.

C. Comparison of Experimental Results on the VAC Sample

After correction for sample length and magnetic field, the difference between the two methods is 16%. The discrepancy is

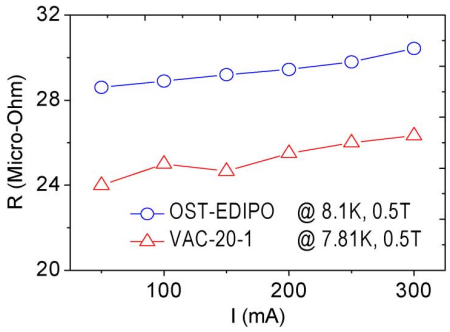

Fig. 6. Inter-filament resistance versus current of OST and VAC samples.

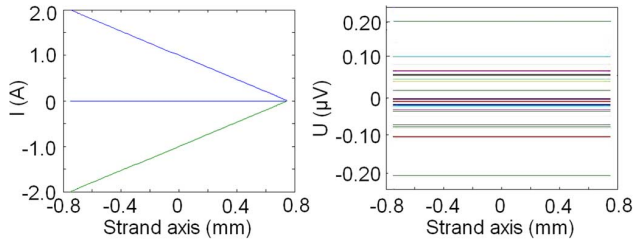

Fig. 7. Filament current and voltage versus axial position, simulated for the VAC wire with the 3D strand model. The current through the unconnected filaments is zero in the longitudinal direction, but not in the radial one.

mainly attributed to the uncertainty in sample length and the local ohmic temperature increase. For a longer second sample ($210\ \mu\mathrm{m}$), the difference between both methods is only 5%.

IV. Simulation and Analysis

A. Simulation Models

Input parameters for the simulations are the independently measured matrix resistivity (RRR), strand geometry, measured current and potential distributions. The outcome of the models is the filament-matrix contact resistivity. First, a FEM based COMSOL model is used for simulation of the low-current measurement. Then, to analyze current distributions including strain and crack influences, a higher-current 3D strand model is developed that also takes into account the superconducting to normal transition. Details of the latter model will be published elsewhere [13].

B. Simulation Results

The simulation result of the VAC NbTi strand is presented. Both current and electrical potential distributions are simulated with the 3D-strand and COMSOL models and are shown in Figs. 7 and 8, respectively. The inter-filament transverse resistivity is much higher than the resistivity of the stabilization matrix. As a result the current density is higher in the matrix than in the filaments, as shown in Fig. 8, or in other words, the filament-to-matrix contact resistance is dominant with respect to the matrix resistance. The outer shell and inner core are preferential paths for the current exchange among filaments [6], [14]. Fig. 9. shows good agreement between the measured inter-filament resistance as a function of magnetic field and the value modeled with a constant filament-to-matrix resistivity.

For wires with thinner filaments ($\mathrm{diameter} \leq 20\ \mu\mathrm{m}$), it is not possible anymore to put two needles on one filament. In this

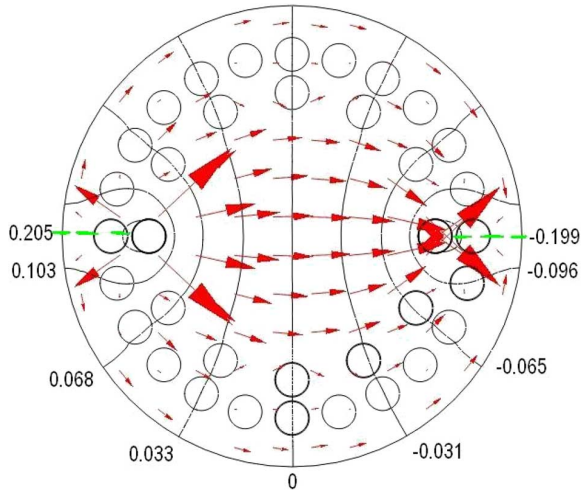

Fig. 8. COMSOL simulation of the transverse current density (arrows) and potential distribution (contours; in $\mu\mathrm{V}$) in the VAC sample.

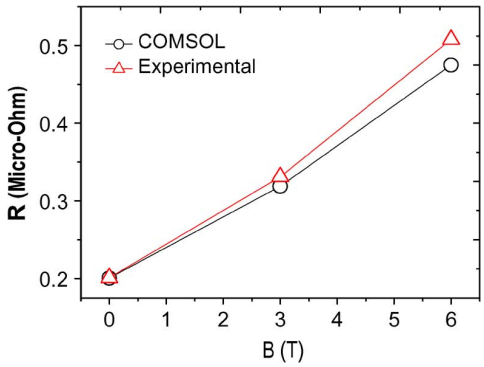

Fig. 9. Comparison between the measured inter-filament resistance of the VAC wire vs. magnetic field and the values simulated with only filament-to-matrix contact resistivity as adjustable parameter (one single value for all fields).

case multifilament contact measurements can not be avoided, which means that several filaments serve as current source and sink just as for the electrical potential distribution in the cross section. The models are used to verify the implications and possible error of such a method. The simulation shows that, except for the region immediately next to the current contacts, current density and electrical potential distribution are similar for single- and multifilament contacts. The agreement between multifilament and two-filament simulations is good. Also the comparison with measured data shows an error of 8% maximum, see Fig. 10. This justifies the application of the multiple contact method in the Point Contact Setup.

For the JT-60-SA strand, the current distribution in matrix and filaments is more uniform than in the VAC wire, as illustrated by comparing Figs. 8 and 11. Because of "current crowding" in between the densely spaced filaments of JT-60-SA, the matrix resistance is increased with respect to the filament-to-matrix contact resistance.

The simulation results of filament-matrix contact resistivity are listed in Table II.

From the combination of experiments and simulations of current and potential distribution, it appears that the filament to matrix contact resistance is larger than the matrix resistance in all investigated wires. This is also confirmed by a simple COMSOL

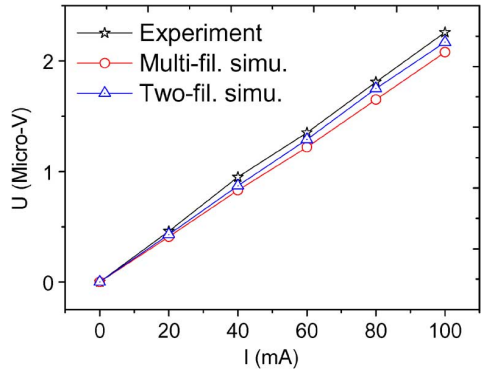

Fig. 10. Comparison of potential drop between same two positions of measured data, two-filament and multi-filaments simulation at 9 K, 0.5 T, 23 μm, sample JT-60-SA.

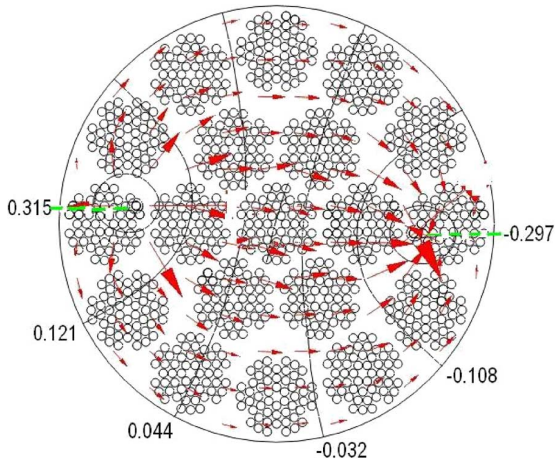

Fig. 11. COMSOL simulation of the transverse current density (arrows) and potential distribution (contours; in μV) in the JT-60-SA sample.

TABLE II
SIMULATION RESULTS

filament-matrix contact resistivity per unit area (Ωm^2)			
Sample	VAC-20-1	JT60SA	OST-EDIPO
COMSOL simulation	1.2×10^{-14}	2×10^{-15}	1×10^{-14}
Numerical 3D strand model	1.4×10^{-14}	3×10^{-15}	Need further development of the model

model for transfer of the contact resisitivity in Ωm^2 into Ωm. Other strand types, presently under investigation show the opposite case.

Both experimental methods are in good agreement, and correspond well with the outcome of both models, providing a good basis for ongoing strand measurements on wire types with small filament diameters. The extracted parameters give a better insight in the crossing current flow pattern, and allow a quantitative description of current redistribution processes inside strands.

V. CONCLUSION

Two different and novel experimental setups for direct interfilament transverse resistance measurement in NbTi and Nb_3Sn multifilamentary wires are developed and results presented. In addition a 3D strand and COMSOL model are developed to study the filament-to-matrix contact resistivity leading to a much better picture of current flow patterns inside strands.

The experimental methods combined with the models provide a solid basis for ongoing strand measurements on wire types with small filament diameters. The extracted parameters allow a quantitative description of current redistribution processes inside strands.

It is foreseen to further optimize the Point Contact Setup and include in the investigations other Nb_3Sn strands with different cross sections of filaments and production techniques.

The 3D numerical strand model will be further developed to analyze current redistribution, strain and crack distributions, as well as, the role of outer matrix sheath, and the change of matrix resistivity in filament zone caused by material diffusion.

REFERENCES

[1] J. W. Ekin, "Current transfer in multifilamentary superconductors. I. Theory," *J. Appl. Phys.*, vol. 49, pp. 3406–3409, 1978.
[2] J. W. Ekin, "Current transfer in multifilamentary superconductors. II. Experimental results," *J. Appl. Phys.*, vol. 49, pp. 3410–3412, 1978.
[3] A. Nijhuis *et al.*, "Impact of spatial periodic bending and load cycling on the critical current of a Nb3Sn strand," *Supercond. Sci. Technol.*, vol. 18, pp. S273–S283, 2005.
[4] B. Turck, M. Wake, and M. Kobayashi, "Transverse resistivity in multifilament superconductive composites," *Cryogenics*, vol. 17, pp. 217–223, Apr. 1977.
[5] K. Ishibashi *et al.*, "Boundary resistance in SC composite wires and cryogenic stability," *Cryogenics*, vol. 19, pp. 161–166, Mar. 1979.
[6] W. Carr, "Longitudinal and transverse field losses in multifilament superconductors," *IEEE Trans. Magn.*, vol. MAG-13, pp. 192–197, 1977.
[7] A. Nijhuis, Y. Ilyin, W. Abbas, and W. A. J. Wessel, "Spatial periodic bending and critical current of bronze and PIT Nb_3Sn strands in a steel tube," *IEEE Trans. Appl. Supercond.*, vol. 17, pp. 2680–2683, 2007.
[8] T. Holúbek, M. Dhallé, and P. Kovác, "Current transfer in MgB2 wires with different sheath materials," *Supercond. Sci. Technol.*, vol. 20, pp. 123–128, 2007.
[9] B. Goldfarb and K. Itoh, "Reduction of interfilament contact loss in Nb3Sn superconductor wires," *16R. J. Appl. Phys.*, vol. 75, pp. 2115–2118, 1994.
[10] V. Corato, L. Muzzi, U. Besi Vetrella, and A. della Corte, "Direct measurement of interfilament resistance in Nb_3Sn strands," *J. Appl. Phys.*, vol. 105, pp. 093930 1–093930 4, 2009.
[11] A. Nijhuis, Y. Ilyin, and W. Abbas, "Axial and transverse stress-strain characterization of the EU dipole high current density Nb3Sn strand," *Supercond. Sci. Technol.*, vol. 21, p. 2008.
[12] M. D. Sumption and E. W. Collings, "Influence of twist pitch and sample length on proximity effect coupling in multifilamentary composites described in terms of a field independent, two current region model," *Cryogenics*, vol. 34, pp. 491–505, 1994.
[13] Y. Miyoshi, E. P. A. van Lanen, C. Zhou, and A. Nijhuis, *to be published*.
[14] B. Turck, "Coupling losses in various outer normal layers surrounding the filament bundle of a superconducting composite," *J. Appl. Phys.*, vol. 50, pp. 5397–5401, 1979.